LAWRENCE
LIVERMORE
NATIONAL
LABORATORY

LLNL-JRNL-410565

Analysis of Geometric Variations in High-Power Tokamak Divertors

M. V. Umansky, R. H. Bulmer, R. H. Cohen, T. D. Rognlien, D. D. Ryutov

February 13, 2009

Nuclear Fusion

Disclaimer

Analysis of geometric variations in high-power tokamak divertors

M.V. Umansky, R.H. Bulmer, R.H. Cohen, T.D. Rognlien, and D.D. Ryutov

LLNL, USA

E-mail: umansky1@llnl.gov

Abstract. Quantitative assessment of performance of high-power tokamak divertors for a range of geometric variations is conducted using the MHD code Corsica (Crotinger et al., Technical report, LLNL, 1997) and edge transport code UEDGE (Rognlien et al. J. Nucl. Materials, 196-198, 347, 1992). In a multi-parametric study the divertor performance is compared for a high-power tokamak with standard and snowflake (Ryutov et al, Phys. Plasmas, 14, 064502, 2007) configurations for the same core plasma parameters. Divertor and edge quantities varied include x-point flux expansion, shape of target plates, and options for the impurity radiation model. For a range of studied cases, in the snowflake the peak heat-load on the target plates is significantly reduced compared to the standard divertor due to larger plasma-wetted area and larger fraction of power radiated in the edge.

PACS numbers: 1315, 9440T

Submitted to:

1. Introduction

Next generation tokamak experiments and fusion reactors such as the proposed Fusion Development Facility (FDF) [1] and the National High-power advanced Torus Experiment (NHTX) [2] will challenge conventional means of peak heat-flux reduction. This makes urgent the search for innovative approaches to the divertor design.
The target plate power flux, q_t, is determined by the power flux from the core into the SOL, P_{LCFS}, the fraction of edge power removed by radiation, f, plasma major radius, R, the power width on the target, L_{pt}, and the target plate pitch angle α (α is zero for the plate orthogonal to the flux surface at the strike point),

$$q_t = (1-f)\frac{P_{LCFS}}{2\pi R_t L_{pt}}\cos\alpha \tag{1}$$

Thus, for given core plasma parameters and power flux there are generally two ways to reduce the target plate heat flux: increasing radiation losses (or other losses, e.g., by charge-exchange neutrals) from the edge region and increasing the plasma-wetted target plate area, $2\pi R_t L_{pt}/\cos\alpha$.
The power width at the target plate, L_{pt}, is set primarily (if the divertor volumetric losses are small) by mapping along flux surfaces,

$$L_{pt} \approx L_{pm}\frac{B_{pm}}{B_{pt}}\frac{R_m}{R_t}, \tag{2}$$

where B_{pm} and B_{pt} are the poloidal field strengths at the mid-plane and at the target plate, respectively; R_m and R_t is the major radius at the mid-plane and at the target plate, respectively. This makes the SOL mid-plane power width, L_{pm}, a key parameter for the heat flux on the target. The mid-plane SOL power width, L_{pm}, results from the balance between the parallel and perpendicular transport in the SOL, which can be expressed as the condition of zero divergence of heat flux, $\nabla\cdot\vec{q}\approx 0$. For conduction-dominated SOL heat flux this gives an estimate of L_{pm},

$$L_{pm} \sim L_c\sqrt{\chi_\perp/\chi_{||}}, \tag{3}$$

where L_c is the connection length and $\chi_\perp$ and $\chi_{||}$ are the effective heat transport coefficients in the perpendicular and parallel directions. Thus the SOL radial heat transport is a key parameter setting the mid-plane power width L_{pm}. Note that in the divertor fanning region the role of radial transport is secondary (see Appendix). The radial transport in the edge is important for the divertor region mainly because it sets the boundary conditions at the entrance into the fanning region.
Designing a high-power divertor requires the knowledge of the SOL power width, L_{pm}. In the absence of a theoretical model that would allow prediction of L_{pm} one has to resort to empirical scalings [3, 4]. One should keep in mind however that empirical scalings are based on present-day machines where the regimes of edge plasma may be very different from future devices.

It seems attractive to find a solution to the divertor heat load problem by inducing strong radiation in the edge. However, to be compatible with the H-mode regime the main edge plasma has to be hot, therefore the edge radiation has to be mainly confined to the divertor volume [5]. Strong radiation from the divertor volume is the basis of the "gas-box" divertor idea where the exhaust energy is removed before reaching the target plate [6]. This "detached" plasma regime usually requires impurity seeding to increase radiative losses, or operating at sufficiently high density [5, 7]. The divertor impurity radiation is certainly helpful for reducing the divertor heat load, however it has limitations; the plasma density for fusion devices is not a free parameter, and impurity ions are not well controlled and confined in the divertor volume. Besides, if the radiating zone is strongly localized near the target plate then about half of radiated energy is still deposited on the plate.

Since the SOL power width, L_{pm}, is not, at present, a controllable parameter this leaves three geometric engineering parameters that can be used for optimizing the divertor: the divertor magnetic flux expansion, target plate major radius, R_t, and the target plate tilt angle α.

Traditionally, the tilt of the target plate, α, is viewed as a main engineering parameter for mitigation of divertor heat flux. However, the angle between the flux surfaces and target plate can not be made arbitrarily small, one reason is that the divertor volume is limited, second comes from limitations on the angle between the total magnetic field and material surface [8].

Increasing the major radius of the target plate, R_t, for mitigating divertor heat load has been proposed in the "super-X divertor" idea [9]. This is an interesting approach that is actively pursued [10].

The recent idea of a "snowflake divertor" [11] exploits a configuration where the flux expansion is much stronger than in the standard x-point divertor. Besides, the snowflake has other properties that may be favorable for heat flux reduction. Construction of magnetic configurations for a tokamak with a snowflake divertor and comparative analysis of snowflake and standard divertors and their effects on the divertor heat flux is the subject of the present study.

2. Snowflake MHD equilibria

2.1. Divertor with 2^{nd} order null

The idea of the "snowflake divertor" proposes to exploit the properties of a 2^{nd} order null point, where both first and second spatial derivatives of the poloidal magnetic flux vanish [11]. Geometrical properties of snowflake divertor are favorable for reducing heat flux on divertor surfaces, due to stronger fanning of the poloidal magnetic flux, larger radiating volume, and larger connection length in the scrape-off layer. Moreover, the stronger shearing of the magnetic field near the null-point may have favorable implications for the SOL plasma turbulence and edge-localized modes (ELMs) [11].

In [11] it has been shown how to construct a 2^{nd} order null in a given magnetic field at a given point by superimposing an additional field to cancel out the 1^{st} and 2^{nd} derivatives of the poloidal magnetic flux. Below we demonstrate another method of constructing a 2^{nd} order null that can be conveniently implemented in a toroidal magnetohydrodynamic (MHD) equilibrium code.

2.2. Construction of 2^{nd} order null

We assume axisymmetric cylindrical geometry. The poloidal magnetic field is described by a flux function $\Psi(x, y)$, where x, y are the radial and vertical cylindrical coordinates. For an exact 2^{nd} (or higher) order null-point the toroidal current j_z must vanish:

$$j_z = \frac{1}{x}\left(\frac{\partial^2\Psi}{\partial x^2} + \frac{\partial^2\Psi}{\partial y^2}\right) + \frac{1}{x^2}\frac{\partial\Psi}{\partial x}, \tag{4}$$

so $j_z = 0$ will be assumed. ‡

It can be shown that a 2^{nd} order null can be constructed by merging together two regular, 1^{st} order x-points. Let P and Q be two regular x-points, Fig. (1). Using auxiliary Cartesian coordinates (ζ, η) such that both P and Q lie on the ζ axis, as shown in Fig. (1), one can define $f(\zeta, \eta) = \partial\Psi/\partial\zeta$. Next, define a coordinate s along the line (P,Q) such that s_P=0 and s_Q=1. The derivative df/ds is

$$\frac{d}{ds}f(s) = \frac{d}{ds}f(\zeta(s), \eta(s)) = \frac{\partial f}{\partial\zeta}\frac{d\zeta}{ds} + \frac{\partial f}{\partial\eta}\frac{d\eta}{ds}, \tag{5}$$

where the second term vanishes since η is independent of s. Since f(s) has roots at s=0 and s=1 then, by the Rolle theorem of calculus [13], there is a point A on the line [P,Q] where df/ds=0 and consequently

$$\frac{\partial f}{\partial\zeta} = \frac{\partial^2\Psi}{\partial\zeta^2} = 0. \tag{6}$$

Now consider function $g(\zeta, \eta) = \partial\Psi/\partial\eta$. Repeating the same argument for $g(\zeta, \eta)$, there is a point B on the line [P,Q] where dg/ds=0 and consequently the cross-derivative of the flux vanishes,

$$\frac{\partial g}{\partial\zeta} = \frac{\partial^2\Psi}{\partial\zeta\partial\eta} = 0. \tag{7}$$

By shrinking the interval [P,Q] and using the condition j_z=0, a point is created where all 1^{st} and 2^{nd} derivatives vanish simultaneously, yielding a 2^{nd} order null-point.

‡ Note that a configuration close to a snowflake, and retaining most of its "good" properties, can be maintained with finite and rather large toroidal current in the divertor region, $j_z \sim 0.1\ I_p/a^2$, where I_p is the total plasma current and a is the plasma minor radius [12].

2.3. Implementation in Corsica code

A self-consistent MHD equilibrium can be constructed with a 2^{nd} order null. We demonstrate this using the Corsica code [14] that solves for axisymmetric MHD equilibrium satisfying the Grad-Shafranov equation and additional constraints, including setting regular x-points at specified locations. This makes it convenient to use the method of merging of two regular x-points to produce a 2^{nd} order null, as described in section (2.2). Figure (2) illustrates a sequence of Corsica equilibria based on the DIII-D tokamak where the secondary x-point approaches the primary one from below. One can observe that as the distance between the two x-points decreases the separatrix acquires the hexagonal shape characteristic of a 2^{nd} order null.

3. UEDGE simulations

3.1. UEDGE model

UEDGE is an axisymmetric edge plasma modeling code solving a system of fluid equations for collisional plasma in the actual toroidal divertor geometry [15]. The radial transport is modeled by ad-hoc transport coefficients usually based on fitting to experimental data, so the UEDGE model is not fully predictive. A specific choice made in the present study for modeling of the radial transport, as described further, follows standard estimates used, for example, for ITER [16]. The present UEDGE calculations are not aiming at modeling plasma edge in a specific device, but rather attempt to analyze generic trends and effects of tokamak divertor geometry. For a different, reasonable, choice of radial transport model the qualitative trends found here would likely be similar.

3.2. Settings used in UEDGE runs

UEDGE simulations are conducted for snowflake-like and standard (1^{st} order null) divertor geometry, with otherwise identically the same parameters, for comparison. The domain is assumed up-down symmetric. The basic plasma parameters and geometry are based on the Fusion Development Facility (FDF) [1]. The major radius is $R \approx 2.5$ m and the input power from the core is set to P=40 MW for the present calculations; in terms of the characteristic P/R ratio this makes it close to ITER and a few times higher than present-day facilities.

The poloidal lengths of divertor legs, L_{pleg}, are matched between the snowflake and standard geometry, and the poloidal field at the strike point is smaller for the snowflake than for the standard configuration, which shows the increased fanning of poloidal flux in the snowflake. All calculations in the present study are conducted with same values of L_{pleg} for inner and outer legs, 0.35 m and 0.39 m, respectively. For the chosen values of L_{pleg} the difference between snowflake and standard configurations in the poloidal field at the outer strike point is about 30%, it would be larger for a shorter leg. The

value of L_{pleg} may be an important parameter affecting the divertor performance, which will be studied in future work.

The radial heat and particle transport is modeled as diffusive, with the inner side coefficients χ=0.1 m^2/s and D=0.1 m^2/s; and the outer side coefficients χ=0.5 m^2/s and D=0.33 m^2/s to represent the ballooning character of the transport. The magnitude of these radial transport coefficients is comparable to that inferred from experimental data for a range of tokamaks [17]. The resulting midplane width of the SOL density and temperature profiles is on the order of 1 cm which is similar to typical tokamak measurments [3].

The level of the in-out asymmetry of the transport coefficients is chosen to produce the in-out power split about 20:80 which is an experimental estimate for the in-out asymmetry in the divertor heat flux in double-null DIII-D discharges [18]. At the core boundary the plasma density is set fixed at 0.7×10^{20} m^{-3}. Impurity radiation from carbon and argon is included using the fixed-fraction impurity model, i.e. $n_Z = \delta_z n_e$, where the impurity fraction δ_z is constant across the domain, and the radiation rates are based on the data from the MIST code [19].

3.3. Six base geometric configurations

Three shapes of the outer target plate are considered: orthogonal plate(α=0°), low tilt (α=45°), and high tilt (α=80°). The shape of the inner target plate for all cases is fixed at $\sim45^0$ tilt. For each target tilt a snowflake and standard x-point cases are considered, thus the total of six geometric configurations, as illustrated in Fig.(3).

3.4. Results for six base configurations

Results from a set of UEDGE runs are summarized below in tables (1) and (2) for the six chosen geometric configurations, for each of them considering three options: no impurity, 1% argon, and 1% carbon. One of the primary figures of merit is the maximum heat flux on the target plates, in particular on the outer plate. Due to the in-out asymmetry of the geometry and transport coefficients most of the heat flux is received by the outer divertor. When the plate tilt is the same for the inner and outer targets, e.g., for cases STD-45 and SNF-45 in Fig.(3), the peak heat flux on the inner target is found to be conideably smaller than that on the outer target. Therefore further only the outer target heat flux is considered.

3.5. Scan of impurity fraction

For the six geometric configurations a scan of impurity fraction is conducted, varying δ_z between 0 and 1%. The plots in Fig. (4) show the maximum power on the outer plate, P_{max}, plotted against δ_z. It is evident from Fig. (4) that in the snowflake configuration the heat flux is considerably (by 30-50%) smaller than in the otherwise similar standard divertor configuration. Besides, the heat flux, clearly depends on the target plate tilt

and the impurity fraction. One can see in Fig. (4) that argon impurity here has much stronger effect than carbon. Note that 1% of fully ionized impurity corresponds to Z_{eff}=1.3 for carbon, and ~ 4.1 for argon.

3.6. Scan of plate tilt angle

To study further the dependence of divertor heat flux on the target plate tilt angle, an additional set of UEDGE runs was conducted varying the target plate tilt, from a plate orthogonal to the magnetic separatrix (or some outward tilt in some cases) to strong inward tilt, reaching the tilt α=80°. The impurity options used for these runs are: no impurity, 1% argon, and 1% carbon. The results are presented in Fig. (5) where P_{max} is plotted against the tilt angle. The plot shows that the heat flux is maximized when the plate is not orthogonal but slightly tilted outwards.

4. Discussion

The data shown in Fig. (5) suggests that there are effects beyond the pure geometry, in particular for nearly orthogonal plate. The mechanism underlying the inward-outward asymmetry of the P_{max} with respect to the plate tilt angle α, apparent in Fig. (5), is in confinement of neutral particles. With outward tilt the neutrals can easier escape the hot plasma region while with inward tilt they are more reflected towards the hot plasma, which in turn results in larger energy losses by radiation and charge-exchange. Similar trends have been observed in AUG divertor experiment and modeling [20].

To capture the geometric effects in a more quantitive way it is convenient to plot P_{max} against the angle γ between the total B field and surface of the target plate at the strike point. As pointed out in [8], for given toroidal field the plasma-wetted area is inversely proportional to γ, and the value of γ is approximately equal to $(B_{pt}/B_{tt})\cos\alpha$, where B_{pt}, B_{tt} are the values of the poloidal and toroidal field on the target. Therefore a linear scaling of P_{max} with γ would indicate geometric effects of increased plasma-wetted area. The plot of P_{max} versus γ is shown in Fig. (6). The values of P_{max} for snowflake and standard configurations tend to be more similar if plotted versus γ than if plotted versus α, as in Fig. (5). Thus the geometry of the plasma-wetted area explains a part of the effect.

However, the data in Fig. (6) display a scaling close to the offset-linear form $P_{max} = A\gamma + B$, where B is the offset value, B $\sim$ 3-5 MW/m^2, indicating that some components of the thermal flux are not governed by the plasma-wetted area geometry. Indeed, the incoming energy flux is dominated by the parallel electron heat conduction but close to the target plate it is partially converted to the ionization energy, P_{iz}, as well as the impurity and hydrogenic radiation power, P_{ir} and P_{hr}; and thermal energy of charge-exchange neutrals, P_{cx}. Some fraction of the power is deposited on the target plate by these channels that do not depend on the target plate tilt in a simple way. In particular referring to the ionization, which is the main component here, the binding

energy ϵ_b =13.6 eV is recovered on the plate via recombination of ions and electrons, $P_{bind} = \Gamma_\perp \epsilon_b$. Here $\Gamma_\perp$ is the normal to the plate particle flux, which has poloidal and radial components

$$\Gamma_\perp = \Gamma_{pol} \cos\alpha + \Gamma_\psi \sin\alpha \tag{8}$$

The radial component, in our model diffusive, $\Gamma_\psi = -D_\perp \partial_\perp n_i$, does not depend on the plate tilt, as long as the radial density profile $n_i(\psi)$ does not change, which explains the presence of the offset B. Of course, for $\gamma \to 0$ the effect of increasing the target surface area would eventually make P_{max} indefinitely small. However there are engineering limitations to how small γ can be made due to the possibility of formation of hot spots on the surface [8].

The data in Fig. (6) show that for given γ, i.e. for plasma-wetted area matched, the target heat flux is still smaller in the snowflake compared to the corresponding standard configuration. This can be attributed to increased connection length and radiative losses in the snowflake.

For given γ, the snowflake has larger flux-tube volume, which leads to larger hydrogen and impurity radiation losses. The plot in Fig. (7) shows the total impurity radiation power for 1% argon impurity plotted vs. γ for standard and snowflake configurations. It is apparent from Fig. (7) that for otherwise similar conditions the radiative losses are larger in the snowflake than in the standard configuration.

The effect of increased connection length is smaller but may also play a role. The connection length L_c, i.e., the distance along magnetic line from the outer midplane to the target is

$$L_c = \int \frac{B}{B_{pol}} dl_{pol}, \tag{9}$$

where l_{pol} is the poloidal distance. Compared to the standard configuration in snowflake the poloidal field is smaller in the vicinity of the null point, which makes the connection length larger. In turn, larger connection length according to Eq. (3) leads to larger mid-plane SOL power width, L_{pm}, which reduces the peak heat flux on the target.

5. Summary and conclusions

In this paper the effects of geometric variations on the performance of a high-power tokamak divertor are analyzed. First, a method of constructing realistic MHD equilibria with the snowflake divertor configuration is demonstrated using the tokamak equilibrium code Corsica. Next, calculations of edge plasma transport are conducted comparing a snowflake divertor against a standard divertor, for same core plasma parameters. The edge transport code UEDGE is used for the calculations, for a range of target plate shapes and impurity radiation options. The results of edge plasma modeling demonstrate that the target plate heat flux is lower for the snowflake than for the standard x-point, due to increased plasma-wetted area and larger fraction of power radiated in the divertor.

6. Appendix

Consider a model where the temperature distribution in divertor volume is governed by the anisotropic heat conduction equation with constant heat conductivities

$$\hat{\chi}_{||}\frac{\partial}{\partial r}(r\frac{\partial T}{\partial r}) + \chi_{\perp}\frac{\partial^2}{\partial r^2}\frac{\partial^2 T}{\partial \theta^2} = 0 \tag{10}$$

The geometry is shown in Fig. (8). The divertor volume where the flux surfaces are fanned is represented by an annular sector with the angular size θ_0, and the poloidal distance is represented by the coordinate r. The poloidal conductivity is $\hat{\chi}_{||} = (B_p/B)^2\chi_{||}$, where B_p is the poloidal field and B is the total field. Use boundary conditions T=0 on the radial sides and at $r = r_2$, and set the temperature $T_1(\theta)$ at the entrance to the divertor, $r = r_1$. The $T_1(\theta)$ profile can be described by a Fourier mode, $T_1 = \sin(n\pi\theta/\theta_0)$, where n is the mode number. Define parameter λ as

$$\lambda = \frac{n\pi}{\theta_0}\sqrt{\frac{\chi_{\perp}}{\hat{\chi}_{||}}} \tag{11}$$

and consider solutions in the form

$$T = \sin(n\pi\theta/\theta_0)R(r) \tag{12}$$

The radial part R(r) obeys

$$r\frac{\partial}{\partial r}(rR') - \lambda^2 R = 0, \tag{13}$$

which has solutions $R \propto r^{\pm\lambda}$, and to satisfy the boundary conditions one should use a linear combination that can be written as

$$R(r) = \frac{\sinh(\lambda\ln(r/r_2))}{\sinh(\lambda\ln(r_1/r_2)}. \tag{14}$$

For any reasonable r_1/r_2 this solution is weakly dependent on λ for small λ, asymptotically

$$R(r) \approx \frac{\ln(r/r_2))}{\ln(r_1/r_2)}\left[1 + \lambda^2\left(\ln^2(r/r_2) - \ln^2(r_1/r_2)\right) + O(\lambda^4)\right] \tag{15}$$

For typical divertor plasma, using for estimate n=3, $\theta_0 = \pi/4$, B_p/B=0.1, and $\chi_{\perp}/\chi_{||} = 10^{-6}$ one finds $\lambda \approx 0.1$, so the distribution of temperature and heat fluxes in the fanning divertor region is only weakly sensitive to the radial heat transport there. Thus, at least in this simple model, the radial transport in the edge is important for the divertor region only in the sense that it sets the boundary conditions at the entrance into the fanning region, the radial transport in the fanning region itself is much less important.

Table 1. Summary of UEDGE runs for standard configurations

	α=0^o	α=45^o	α=80^o
B_{pol} [T]	0.66	0.66	0.64
B_{tor} [T]	6.5	6.4	6.6
B_{pol}/B_{tor}	0.1	0.1	0.1
$\cos\alpha$	1.0	0.6	0.16
γ	0.1	0.06	0.015
No imp. P_{max} $[MW/m^2]$	80.	55.	16.
1% C P_{max} $[MW/m^2]$	77.	44.	10.
1% Ar P_{max} $[MW/m^2]$	25.	21.	10.

Table 2. Summary of UEDGE runs for snowflake configurations

	α=0^o	α=45^o	α=80^o
B_{pol} [T]	0.5	0.5	0.5
B_{tor} [T]	6.4	6.4	6.3
B_{pol}/B_{tor}	0.08	0.08	0.08
$\cos\alpha$	1.0	0.65	0.17
γ	0.08	0.05	0.014
No imp. P_{max} $[MW/m^2]$	50.	30.	11.
1% C P_{max} $[MW/m^2]$	23.	23.	10.
1% Ar P_{max} $[MW/m^2]$	14.	13.	7.

Figure 1.

P and Q are two standard, 1^{st} order x-points. Auxiliary coordinates (ζ,η) are set up so that point P is at ζ=0,η=0 and point Q lies on the ζ axis.

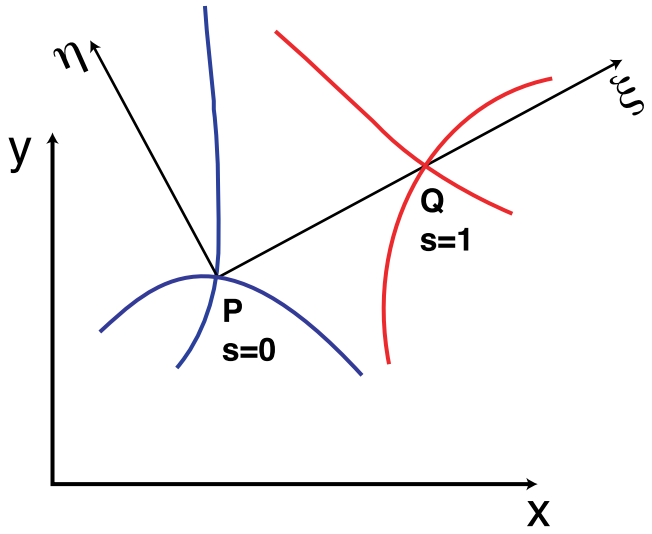

Figure 2.

Flux surfaces for a sequence of Corsica solutions based on the DIII-D tokamak where the secondary x-point approaches the primary one from below. The x-points are shown in circles. Shown cases correspond to the the distance between x-points (a) 30 cm, (b) 20 cm, (c) 10 cm, and (d) 5 cm. In case (d) the separatrix has the characteristic hexagonal shape.

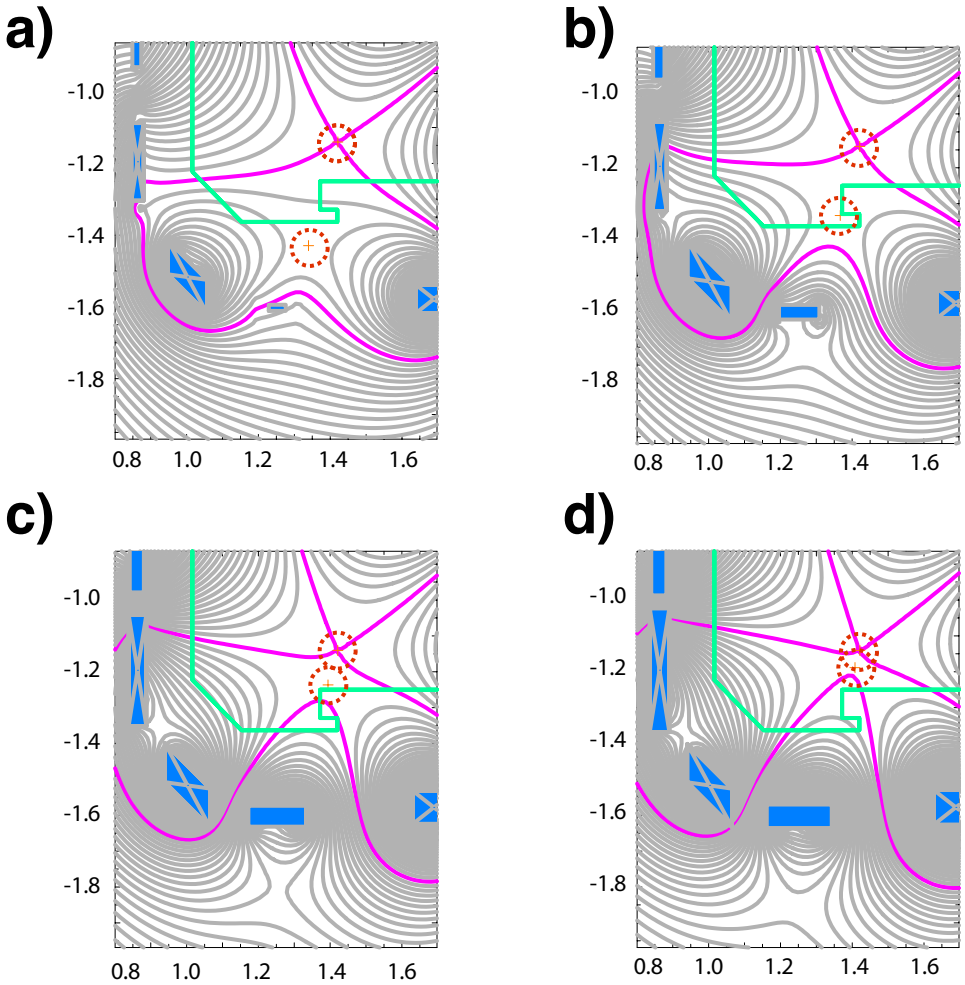

Figure 3.

Computational mesh for the six base configurations, standard (top) and snowflake (bottom), illustrating the geometry used in the UEDGE simulations. The target plates are at poloidal boundaries of the domain, as shown in the top middple plot. The outer plate tilt angle is (left to right) $\alpha = 0^0$, $\alpha = 45^0$, and $\alpha = 80^0$. The tilt of the inner plate is $\sim 45^0$ in all cases.

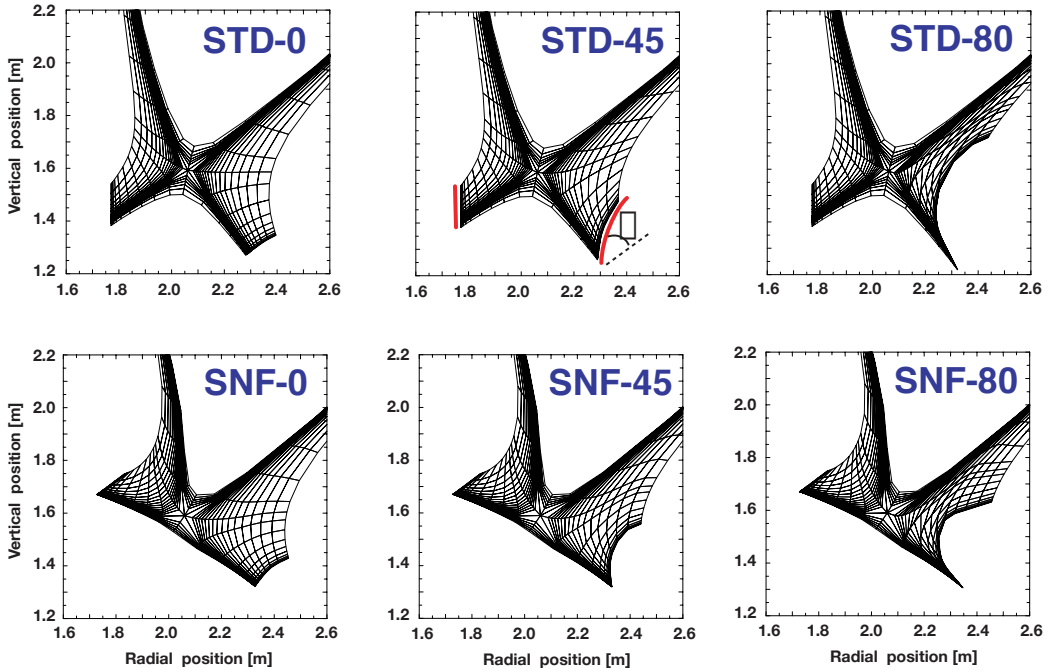

Figure 4.

The maximum heat flux on the outer target plate plotted vs. the impurity fraction. Different curves correspond to the six base geometry cases in Fig. (3), as labeled. The shaded area at the bottom corresponds to the heat flux below 10 MW/m^2.

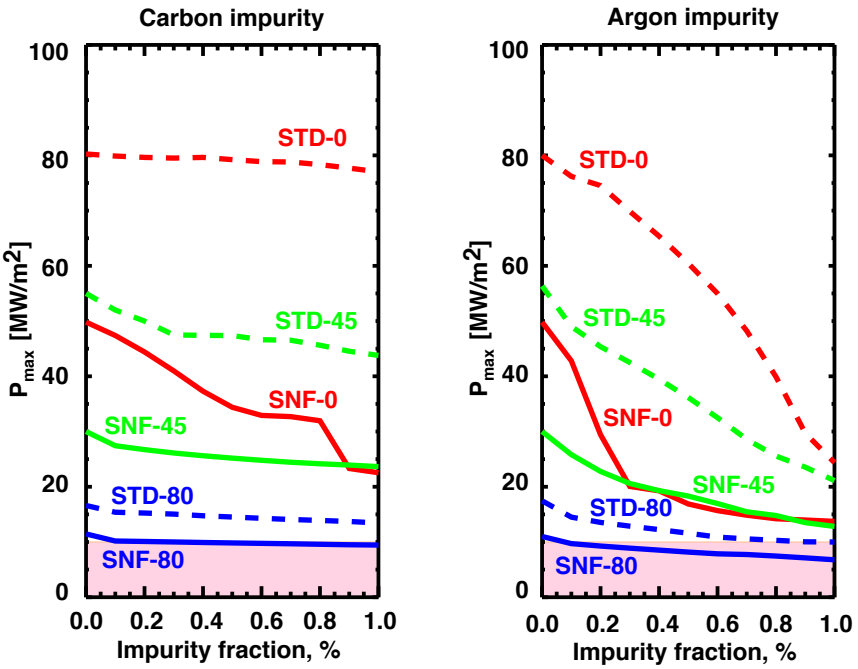

Figure 5.

The maximum heat flux on the outer target plate is plotted vs. the plate tilt angle α. Negative sign corresponds to inward tilt, positive sign to outward tilt. Different curves correspond to snowflake and standard configurations with 1% argon, 1% carbon, as labeled.

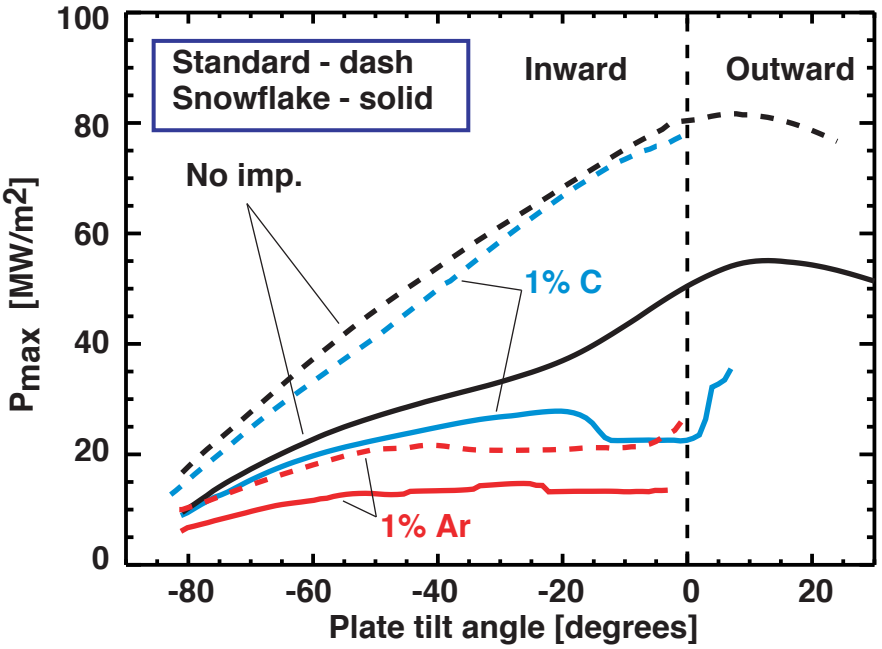

Figure 6.

The maximum heat flux on the outer target plate is plotted vs. the total angle γ between the magnetic vector and the target plate surface at the strike point. Different curves correspond to snowflake and standard divertor cases with no impurity, 1% argon, 1% carbon, as labeled. The shaded area at the bottom corresponds to heat flux below 10 MW/m^2. The vertical dashed line shows $\gamma = 1^0$ which may be the practical limit (see main text).

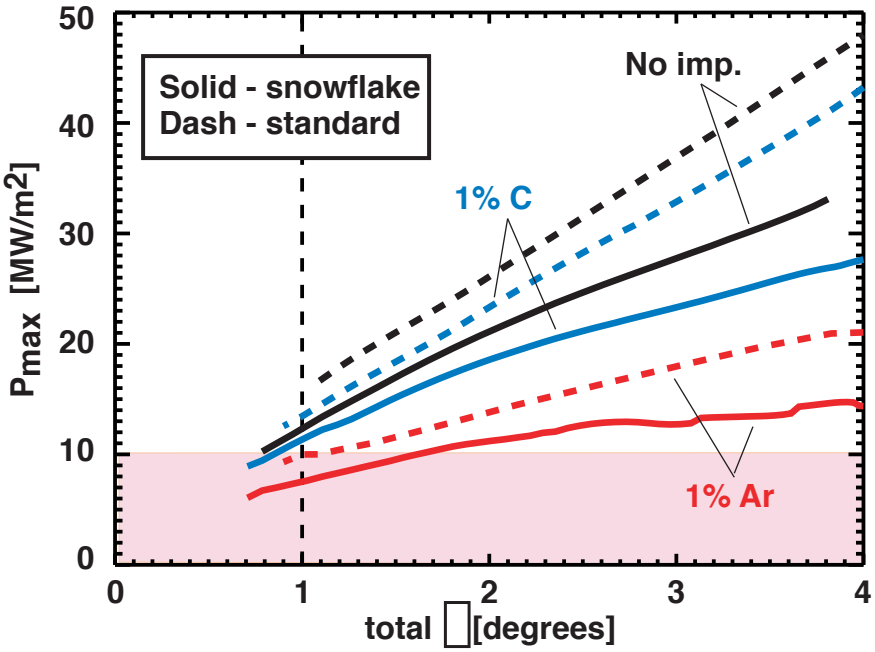

Figure 7.

Total, integrated over the domain volume, impurity radiation power, P_{irad}, plotted vs. the angle γ for 1% argon impurity. For given γ the value of P_{irad} for snowflake is larger than for corresponding standard divertor. Input power into the edge is 40 MW.

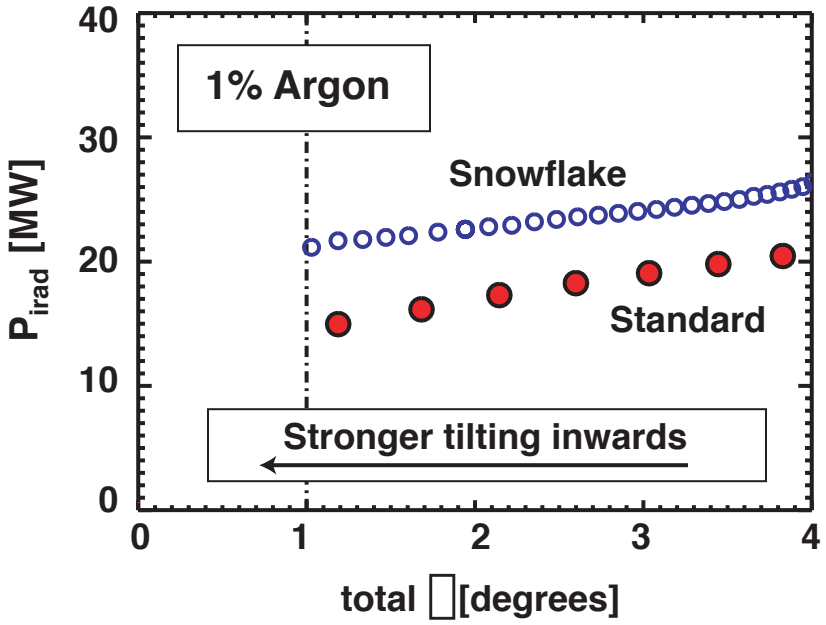

Figure 8.

(a) The edge domain includes the external part of the core region, the scrape-off layer (SOL), and the private flux (PF) region. (b) Ihe SOL can be schematically represented by the main SOL region (above the x-point) and the region near the x-point where magnetic surfaces are fanned out. (c) The fanning region can be represented by an annular sector with angular size $[0,\theta_0]$ and radial size $[r_1,r_2]$.

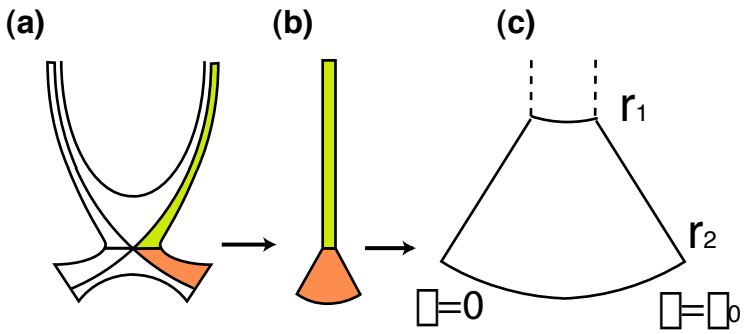

Acknowledgments

This work was performed under the auspices of the U.S. Department of Energy by Lawrence Livermore National Laboratory under Contract DE-AC52-07NA27344.

References

[1] Stambaugh R. D. The fusion development facility. http://web.gat.com/fdf/, 2007.

[2] Goldston R. J. et al. An experiment to tame the plasma material interface. In *22nd IAEA Fusion Energy Conference*, Geneva, Switzerland, October 2008. IAEA. FT/P3-12.

[3] McCormick K. et al. *J. Nucl. Materials*, 266-269:99–108, 1999.

[4] Kallenbach I. et al. *J. Nucl. Materials*, 337-339:381–385, 2005.

[5] Stambaugh R. et al. *Nuclear Fusion*, 39:2391, 1999.

[6] Rebut P-H. et al. *Fusion Engineering and Design*, 22:7–18, 1992.

[7] Vlases G. et al. *J. Nucl. Materials*, 241-243:310–315, 1997.

[8] Ryutov D. D. et al. A snowflake divertor: a possible way of improving the power handling in future fusion facilities. In *22nd IAEA Fusion Energy Conference*, Geneva, Switzerland, October 2008. IAEA. IC/P4-8.

[9] Kotschenreuther M. et al. *Physics of Plasmas*, 14:072502, 2007.

[10] Kotschenreuther M. et al. The super x divertor (sxd) and high power density experiment (hpdx). In *22nd IAEA Fusion Energy Conference*, Geneva, Switzerland, October 2008. IAEA. IC/P4-7.

[11] Ryutov D. D. *Physics of Plasmas*, 14:064502, 2007.

[12] Ryutov D. D. A snowflake divertor and its properties. In *34th EPS Conference on Plasma Phys.*, Warsaw, Poland, July 2007. D-1.002.

[13] Apostol T. M. *One-Variable Calculus, with an Introduction to Linear Algebra*. Blaisdell, 1967.

[14] Crotinger J. A. Corsica:a comprehensive simulation of toroidal magnetic-fusion devices. Technical report, LLNL, 1997. UCRL-ID-126284.

[15] Rognlien T. D. et al. *J. Nucl. Materials*, 196-198:347, 1992.

[16] Kukushkin A. S. et al. *J. Nucl. Materials*, 337-339:50–54, 2005.

[17] Porter G. D. et al. *J. Nucl. Materials*, 266-269,:917–921, 1999.

[18] Petrie T. private communication, 2008.

[19] Hulse R. A. *Nuclear Technology - Fusion*, 3:259, 1983.

[20] Schneider R. et al. *Contrib. Plasma Phys.*, 1-2:3–191, 2006.